Microstructure and magnetic properties of Fe/Ti multilayers

1997 J. Phys.: Condens. Matter 9 103

(http://iopscience.iop.org/0953-8984/9/1/012)

J. Phys.: Condens. Matter **9** (1997) 103–115. Printed in the UK PII: S0953-8984(97)76043-0

Microstructure and magnetic properties of Fe/Ti multilayers

M Kopcewicz†§, T Stobiecki‡, M Czapkiewicz‡ and A Grabias†

† Institute of Electronic Materials Technology, Wólczyńska 133, 01-919 Warszawa, Poland
‡ Department of Electronics, University of Mining and Metallurgy, Al. Mickiewicza 30, 30-059 Kraków, Poland

Received 8 July 1996, in final form 19 August 1996

Abstract. The microstructure and magnetic properties of Fe/Ti multilayer films prepared by rf-sputtering deposition are studied via conversion electron Mössbauer spectroscopy (CEMS), x-ray diffraction (XRD), and magnetic techniques. Samples with the two Ti-to-Fe thickness ratios $\beta = 1$ and $\beta = 1.5$, and with modulation wavelengths of 5 to 80 nm were studied. The XRD, electrical conductivity and coercive-field measurements revealed that the amorphous phase is formed during deposition and is distributed in the plane between the crystalline sublayers as well as in the grain boundaries. From CEMS measurements the relative fractions of the various phases (α-Fe, the interfacial FeTi crystalline phase and the amorphous phase) were determined. The thickness of the mixed interfacial region was estimated for various values of Λ and β. The CEM spectra revealed that the spins in the Fe sublayers are aligned in the plane of the film, while in the interfacial regions they are randomly oriented. It is shown that the films with $\Lambda = 5$ nm are almost entirely amorphous. The relative fraction of the amorphous phase decreases dramatically with increasing Λ.

1. Introduction

Artificially composition-modulated materials whose microstructure and magnetic properties depend strongly on the thickness of the individual elemental layers have been attracting considerable attention in recent years. A good example of such materials is the Fe/Ti system which is interesting both from the point of view of basic research and because of its applications (e.g. as a buffer layer in the multilayer structure for a giant-magnetoresistance (GMR) sensor [1] and as a hydrogen-storage material [2, 3]). Another material studied extensively is the Fe/Zr system which reveals considerable similarities as well as distinct differences when compared to the Fe/Ti system with a corresponding range of layer thicknesses. Recently, systematic studies of the microstructure of the Fe/Zr multilayer system, including the structural transformation from the predominantly crystalline to the almost completely amorphous state induced by ion-beam mixing, were performed [4, 5].

Under equilibrium conditions the bulk Fe–Ti system exists either as a crystalline intermetallic compound or as an amorphous alloy. The only crystalline intermetallic compounds known of are bcc-Fe(Ti) and hcp-Fe_2Ti [6, 7]. However, because of the low solubility of Ti in Fe (a few per cent) only the iron-rich crystalline FeTi alloy with the bcc structure can be formed [8, 9]. The solubility range can be extended to about 20% by fast

§ Author to whom any correspondence should be addressed; e-mail: kopcew_m@sp.itme.edu.pl; fax: 48 39120764.

0953-8984/97/010103+13$19.50

quenching [9]. The amorphous Fe_xTi_{1-x} phase can be produced over a wide composition range ($0.25 \leqslant x \leqslant 0.80$) by vapour-quenching or sputtering deposition [10–13]. However, the melt-quenching technique, commonly used for the production of numerous amorphous alloys, does not produce FeTi alloys in the amorphous state [14]. The FeTi alloys prepared by splat cooling from the melt are either the β-Ti(Fe) or TiFe(Ti) solid solutions with a solubility range extended up to 50% [15]. Very different structural and magnetic properties and hyperfine interactions have been observed for the amorphous FeTi state as compared with crystalline alloys and compounds [10, 11].

It is fairly easy to distinguish the amorphous FeTi phase from the crystalline FeTi and Fe_2Ti compounds thanks to the clearly different quadrupole splittings and isomer shifts of the latter [10–13, 16]. As shown in references [10] and [11], the quadrupole splitting (QS) depends strongly on the iron content in amorphous Fe_xTi_{1-x} alloys for $x < 0.6$ and decreases almost linearly from about 0.36 mm s^{-1} to 0.29 mm s^{-1} for $x \approx 0.25$ and 0.6, respectively. The QS value remains almost constant for $x \approx 0.6$–0.7 and then increases again to about 0.31 mm s^{-1} for $x \approx 0.8$. The isomer shift (δ) is less sensitive to the alloy composition. It increases from about -0.22 mm s^{-1} for $0.25 \leqslant x \leqslant 0.5$ to about -0.15 mm s^{-1} for $x \approx 0.8$. The bcc-Fe(Ti) alloy is magnetic with a hyperfine field of about 29 T and $\delta \approx 0.02$ mm s^{-1} at room temperature. The formation of such a bcc-Fe(Ti) alloy as a result of Ti-ion implantation into α-Fe has been observed recently [17].

The microstructure and magnetic properties of the Fe/Ti multilayer system depend strongly on the thicknesses of the individual Fe and Ti layers (d_{Fe} and d_{Ti}), the structural modulation wavelength $\Lambda = d_{Fe} + d_{Ti}$ and the composition of the system determined by the thickness ratio of the Ti and Fe layers $\beta = d_{Ti}/d_{Fe}$.

In this paper we have studied a Fe/Ti multilayer system prepared by rf-sputtering deposition. Samples with two nominal compositions were prepared: $Fe_{0.5}Ti_{0.5}$ ($\beta = 1.5$) and $Fe_{0.6}Ti_{0.4}$ ($\beta = 1$). The modulation wavelength ranged from 5 nm to 80 nm for both compositions. The structural properties of the Fe/Ti system were studied with respect to Λ and β via Mössbauer spectroscopy (the conversion electron technique, CEMS) and x-ray diffraction (XRD). The magnetic properties were investigated via the CEMS technique and via conventional magnetic measurements (hysteresis loop, magnetoresistivity).

2. Experiment

Multilayer Fe/Ti films were prepared by rf-sputtering deposition by using Fe and Ti targets at a base pressure of 1×10^{-5} Pa. The pressure during the sputtering of the argon gas was 0.7 Pa and the deposition rates were 0.6 nm s^{-1} and 0.5 nm s^{-1} for Fe and Ti, respectively. Samples with the two thickness ratios $\beta = d_{Ti}/d_{Fe} = 1.5$ (nominal composition $Fe_{0.5}Ti_{0.5}$) and $\beta = 1$ ($Fe_{0.6}Ti_{0.4}$) were prepared. The elemental thicknesses of the Fe and Ti layers were 2.5, 5, 10, 20, 30 and 40 nm for $\beta = 1$, and 2, 4, 8, 16, 24 and 32 nm of Fe and 3, 6, 12, 24, 36 and 48 nm of Ti for $\beta = 1.5$. Thus, the modulation wavelengths $\Lambda = d_{Fe} + d_{Ti}$ varied from 5 to 80 nm for both compositions. The total thickness of the film stacks deposited on Corning glass was about 240 nm. The thickness of the elemental layers was measured during deposition with a quartz sensor with an accuracy of ± 0.2 nm.

The microstructure of the Fe/Ti multilayers was characterized by CEMS and XRD. The CEMS measurements were performed at room temperature by using a He–6% CH_4 gas-flow electron counter. A computer-controlled spectrometer with a ^{57}Co-in-Rh source was used. The isomer shifts are given with respect to the α-Fe standard. The Mössbauer spectral parameters (hyperfine fields, H_{hf}, quadrupole splittings, QS, and isomer shifts, δ) were obtained by fitting Lorentzian line shapes to the experimental data by the least-squares

method. The calculations of the quadrupole-splitting distribution $P(\mathrm{QS})$ were performed by using the constrained Hesse–Rübartsch method (see [18, 19]). The NORMOS program was used.

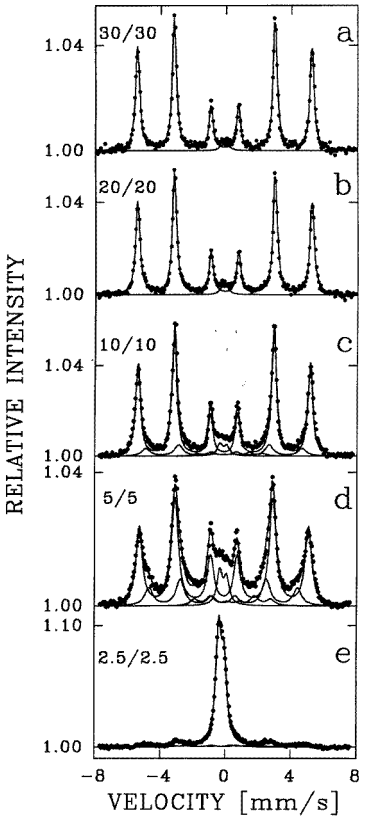

Figure 1. CEM spectra obtained for Fe/Ti multilayers with $\beta = 1$. The elemental layer thicknesses are given.

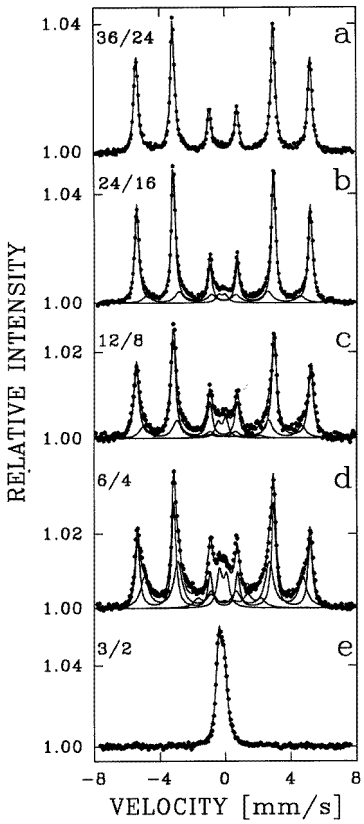

Figure 2. CEM spectra obtained for Fe/Ti multilayers with $\beta = 1.5$. The elemental layer thicknesses are given.

The XRD measurements were carried out in the Bragg–Brentano geometry by using Co Kα radiation. The magnetoresistivity and the magnetic hysteresis loop were measured at room temperature for the samples prepared simultaneously in the same deposition process as those for CEMS experiments. These studies were supplemented by electrical conductivity measurements.

3. Results and discussion

3.1. The Mössbauer studies

The properties of Fe/Ti multilayers with modulated atomic (crystalline/amorphous) and magnetic structures (ferromagnetic/paramagnetic) depend strongly on the thickness of each constituent. The conversion electron Mössbauer (CEM) spectra clearly reveal this dependence. In figures 1 and 2 the CEM spectra recorded for Fe/Ti multilayers with $\beta = 1$

and $\beta = 1.5$, respectively, and for a decreasing modulation wavelength Λ are shown. As can be seen the multilayer films with $\Lambda \geqslant 60$ nm are almost completely crystalline (figures 1(a), 2(a)). The CEM spectra consist of the magnetic-hyperfine-split sextet with the hyperfine field $H_{hf} \approx 32.8$ T and isomer shift $\delta = 0.00$ mm s^{-1} characteristic for α-Fe at room temperature. H_{hf} is slightly reduced as compared with the value for bulk α-Fe; this is related to the stresses in the film. Traces (about 2% of the total spectral area) of the quadrupole doublet (QS) can be detected for $\Lambda = 60$ nm and $\beta = 1$ (figure 1(a)). The QS doublet corresponds to the amorphous FeTi phase formed during deposition at the interfaces between Fe and Ti layers.

The relative amount of the amorphous FeTi phase rapidly increases with decreasing Λ as revealed by the increase of the spectral contribution of the QS doublet. For $\Lambda = 20$ nm and both film compositions (figures 1(c), 2(c)) the CEM spectra consist of a QS doublet (QS ≈ 0.40 mm s^{-1} and $\delta \approx -0.09$ mm s^{-1}) and three magnetically split components: (i) that corresponding to α-Fe ($H_{hf} = 32.8$ T, $\delta = 0.00$ mm s^{-1}), (ii) that corresponding to the bcc-Fe(Ti) alloy formed at the interface ($H_{hf} = 28.5$–29.9 T, $\delta \approx 0.00$ mm s^{-1}), and (iii) that corresponding to the Fe atoms in the interface with Ti atoms in the vicinity, which reduce H_{hf} to about 12 T ($\delta \approx 0.35$ mm s^{-1}). The quadrupole splitting of about 0.40 mm s^{-1} suggests that the amorphous phase is iron-poor [10, 11]. A similar shape of the CEM spectra was observed for $\Lambda = 10$ nm (figures 1(d), 2(d)). In this case the relative spectral contribution of the QS doublet and the magnetic sextets with $H_{hf} \approx 29$ T and $H_{hf} \approx 12$ T markedly increase at the expense of the α-Fe sextet. The multilayers with the smallest modulation wavelengths ($\Lambda = 5$ nm for both $\beta = 1$ and $\beta = 1.5$) are almost completely amorphous. The CEM spectra consist of a dominating quadrupole doublet (figures 1(e), 2(e)). The value QS ≈ 0.33 mm s^{-1} determined for this doublet by fitting two Lorentzian lines with the linewidth of 0.4 mm s^{-1} corresponds to the Fe_xTi_{1-x} amorphous phase with $x \approx 0.4$–0.5 [10, 11]. The residual magnetic-hyperfine-split component with two characteristic magnetic hyperfine fields of 29.9 T and 13.5 T contributing to about 18% of the total spectral area is clearly seen for $\beta = 1$ (figure 1(e)). The spectrum recorded for the $\beta = 1.5$ and $\Lambda = 5$ nm film shows that this film is almost entirely amorphous (figure 2(e)). Traces of the magnetic component contribute to less than 3% of the spectral area.

From the magnetically split spectral component corresponding to the Fe layer and interfacial FeTi components (figures 1(a)–1(d) and 2(a)–2(d)) it is possible to determine the spin orientation in the multilayer system with respect to the γ-ray direction. In all of the Mössbauer measurements the γ-rays were perpendicular to the plane of the sample. In the general case the line intensity ratio in the Zeeman sextet is 3:α:1:1:α:3, where

$$\alpha = \frac{4\sin^2\Theta}{1+\cos^2\Theta} \tag{1}$$

(Θ is the angle between the direction of the hyperfine field H_{hf} and the propagation direction of the gamma rays). The parameter α varies from 0 to 4 depending on Θ. For instance, $\alpha = 0$ for $\Theta = 0^\circ$ (H_{hf} parallel to the γ-ray direction, i.e. the spins are perpendicular to the plane of the sample), $\alpha = 4$ for $Q = 90^\circ$ (the spins are aligned in the plane of the sample), and $\alpha = 2$ for random spin orientation. In most of the cases shown in figures 1 and 2 the parameter α is close to 4 in the subspectrum corresponding to the α-Fe phase, which shows that the spins are aligned predominantly in the plane of the film. However, in the spectral components corresponding to the FeTi interfacial regions $\alpha \approx 2$ which suggests random spin orientation at the interfaces.

For the films with $\Lambda = 5$ nm the CEM spectra were measured over a reduced velocity range which allowed the quadrupole-splitting distributions to be extracted (figure 3).

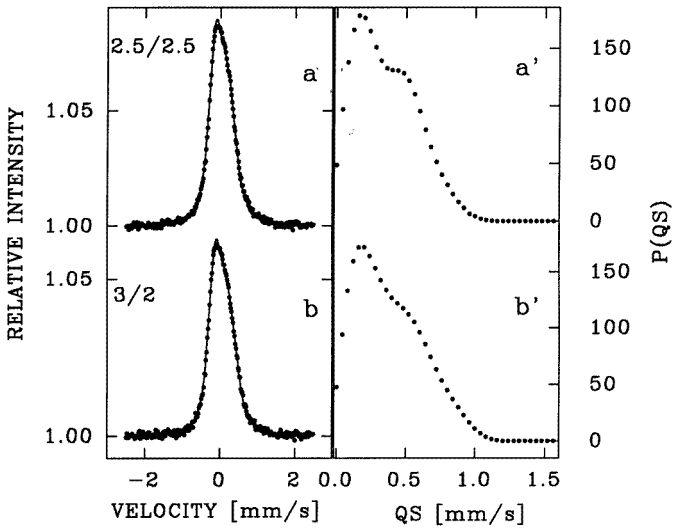

Figure 3. CEMS analysis of the amorphous phase with a reduced velocity range. The solid line passing through the data points ((a), (b)) is the result of the fit of a quadrupole-splitting distribution P(QS) ((a′), (b′)).

The quadrupole-splitting distributions, P(QS), were extracted from the CEM spectra (figures 3(a), 3(b)) by using the constrained Hesse–Rübartsch method (see [18, 19]). A linear correlation between the isomer shift and the quadrupole splitting was assumed, as the first approximation in the calculations. P(QS) consists of two quite distinct peaks (figures 3(a′), 3(b′)). Similar structure in P(QS) was observed recently for the Fe/Zr multilayer system which was amorphized due to ion-beam mixing [5]. The complex shape of the P(QS) distribution was attributed to the phase separation in the amorphous $Fe_{100-x}Zr_x$ system. This interpretation was based on a model which predicts the local maximum in the free-energy curve of the amorphous $Fe_{100-x}Zr_x$ system at $x \approx 50$ and suggests that amorphous phases with the Fe-to-Zr ratios of 1:2 and 2:1 are more stable and therefore more likely to appear [20]. The composition modulation in the amorphous phase was also detected by the small-angle x-ray diffraction technique an the earlier study of the Fe/Zr multilayer system amorphized due to solid-state reaction [4]. The shape of P(QS) observed in figures 3(a′) and 3(b′) suggests that the amorphous FeTi phase is inhomogeneous and consists of layers with high and low iron content.

The spectral contribution of the QS doublet corresponding to the amorphous FeTi phase depends on the thickness of the Fe layer. The relative amorphous fractions versus d_{Fe} and versus Λ for both film compositions are shown in figures 4(a) and 4(b). As can be seen, the spectral contribution related to the amorphous phase continuously decreases with increasing d_{Fe} and Λ, but for a given Λ it is usually higher for the Ti-rich ($\beta = 1.5$) system (figure 4(b)).

The amorphous phase is formed during the rf-sputtering deposition process at the interfaces. Thus, because of the decreasing number of interfaces in the samples with large Λ, the relative amount of Fe atoms belonging to the amorphous phase and to the interfacial regions is too small to be detected by CEMS.

The relative fractions ΔF of the various phases—α-Fe, interfacial FeTi and amorphous FeTi—formed during the deposition process are given in table 1. From these values one can

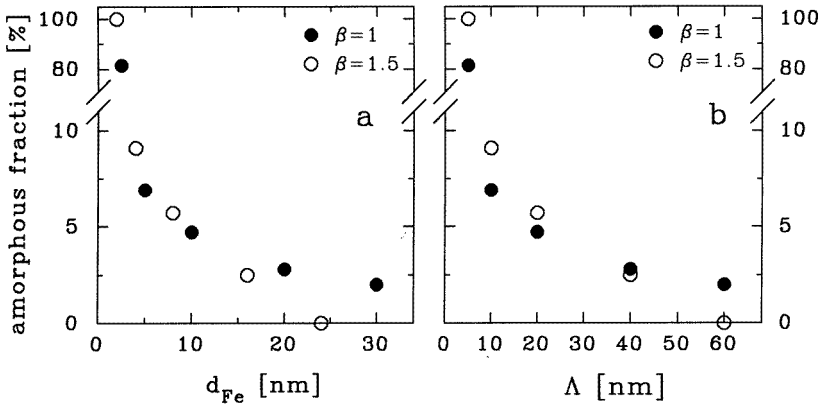

Figure 4. The relative abundance of the amorphous phase versus iron layer thickness d_{Fe} (a) and the modulation wavelength Λ (b).

Table 1. Relative fractions of the various phases—α-Fe, interfacial FeTi ($H_{hf} \approx 29$ T and 12 T) and amorphous FeTi—determined from CEMS measurements.

		Relative fraction of a given phase (ΔF) (%)			
			Interfacial FeTi		
$d_{\mathrm{Ti}}/d_{\mathrm{Fe}}$ (nm)	Λ (nm)	α-Fe	29 T	12 T	Amorphous FeTi
2.5/2.5	5	—	14	5	81
5/5	10	68	19	6	7
10/10	20	81	12	3	4
20/20	40	97	—	—	3
30/30	60	98	—	—	2
40/40	80	100	—	—	—
3/2	5	—	—	—	100
6/4	10	45	37	9	9
12/8	20	70	20	4	6
24/16	40	81	16	—	3
36/24	60	100	—	—	—
48/32	80	100	—	—	—

estimate the average thickness of the iron layer converted into the amorphous or interfacial FeTi phases. The mixed-layer thickness is [4, 21]

$$\Delta x = nd\,\Delta F/2 \tag{2}$$

where n is the number of monolayers of Fe per Fe–Ti bilayer, $d = 0.203$ nm is the d-spacing in the Fe layers (i.e. the Fe monolayer thickness), ΔF is the spectral area fraction of a given phase and the factor 2 accounts for there being two Fe–Ti interfaces per Fe layer. The density differences and possible differences in the recoilless fractions for α-Fe and the amorphous and interfacial FeTi phases are neglected. The thickness of the Fe layer converted into the interfacial FeTi phase (29 T and 12 T components) for $\beta = 1$ multilayers estimated in this way is about 0.65 nm (per interface) for the 5/5 nm film and 0.75 nm for the 10/10 nm one. In the 2.5/2.5 nm film a $\simeq$1.02 nm thick (per interface) iron layer is

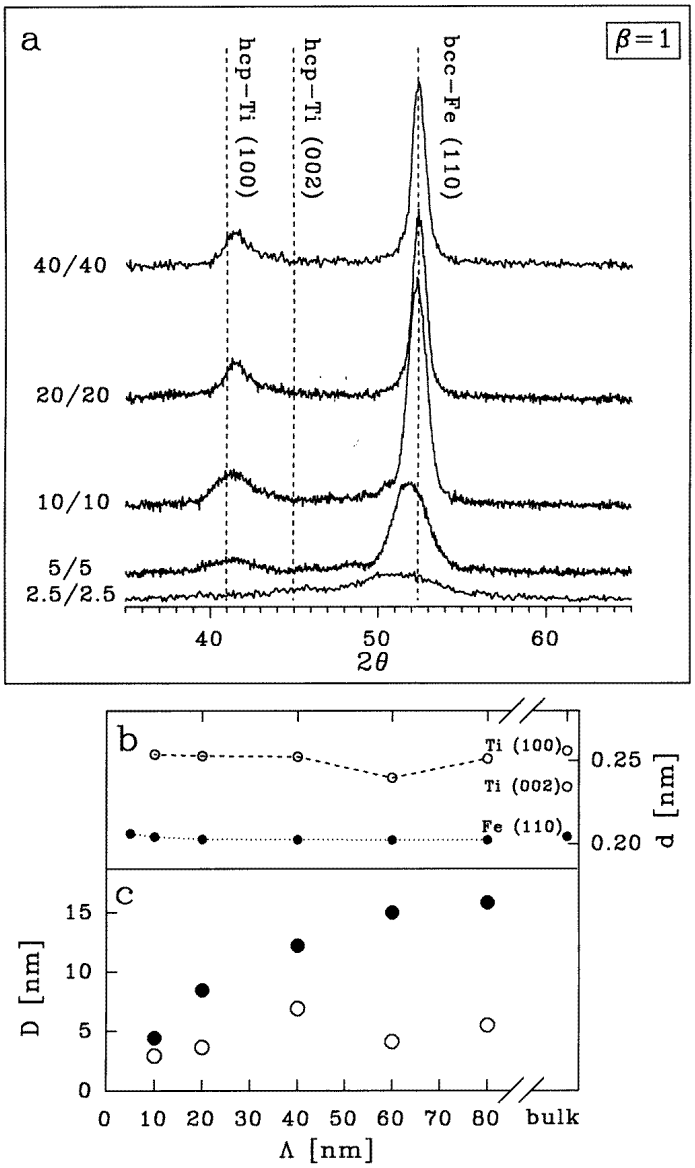

Figure 5. XRD patterns of the FeTi multilayers with different sublayer thicknesses for $\beta = 1$ (a). The dashed lines correspond to the positions of the bulk bcc-Fe (110), hcp-Ti (100) and hcp-Ti (002) diffraction peaks. The d-spacing (b) and the size, D, of the Ti and Fe crystallites (c) versus Λ are shown.

consumed for the formation of the amorphous phase. In the $\beta = 1.5$ systems slightly thicker Fe layers are converted to form the interfacial FeTi phase (about 0.92 nm per interface for the 6/4 nm film and about 0.96 nm per interface for the 12/8 nm one).

The CEMS results obtained for the Fe/Ti multilayers show a great similarity to those recently obtained for the Fe/Zr multilayer system with comparable modulation wavelengths and average compositions [5]. The amorphous and interfacial phases appear for similar

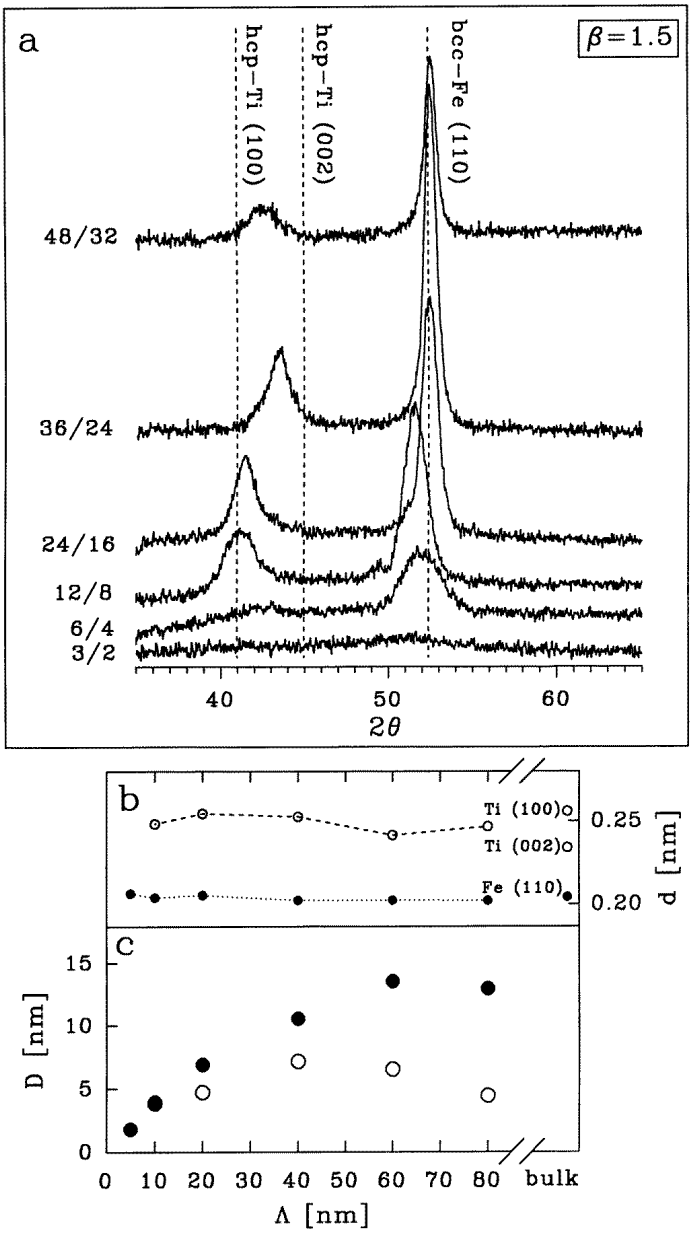

Figure 6. XRD patterns of the FeTi multilayers with different sublayer thicknesses for $\beta = 1.5$ (a). The dashed lines correspond to the positions of the bulk bcc-Fe (110), hcp-Ti (100) and hcp-Ti (002) diffraction peaks. The d-spacing (b) and the size, D, of the Ti and Fe crystallites (c) versus Λ are shown.

values of Λ in the two systems. However, the amorphous phase is more abundant in the Fe/Ti systems with small Λ ($\Lambda = 5$ nm) than in the corresponding Fe/Zr one; the amorphous phases contribute to about 97% and 35% of the total spectral area for the Fe/Ti and Fe/Zr systems ($\beta = 1$, $\Lambda = 5$ nm), respectively. This finding is a little surprising, because the heat

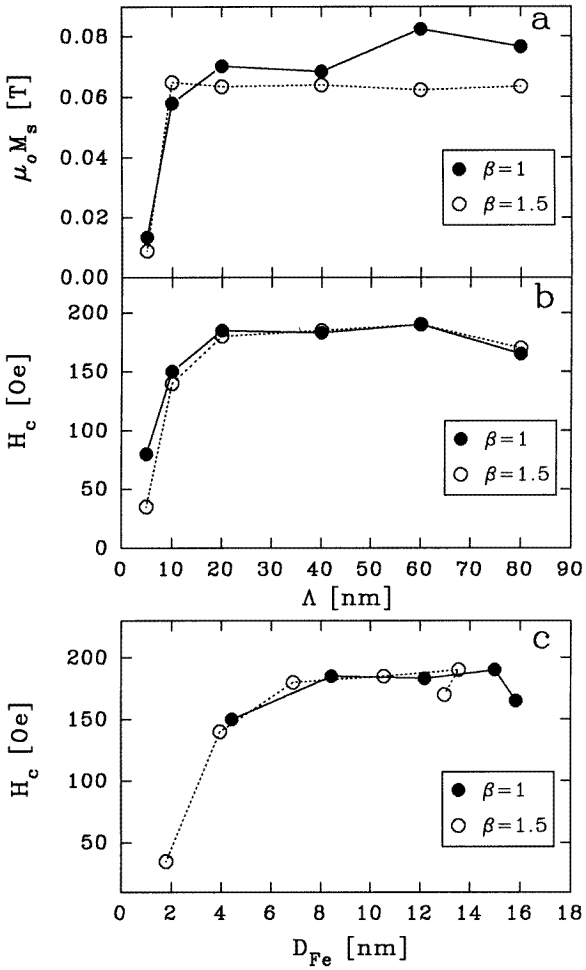

Figure 7. The magnetization and coercive field H_c versus modulation wavelength Λ for $\beta = 1$ and $\beta = 1.5$ are shown in (a) and (b), respectively, and H_c versus Fe grain size D_{Fe} is shown in (c).

of formation of the amorphous phase is larger for the Fe/Zr system ($\Delta H_{max} = -25$ kJ mol^{-1}) than for the Fe/Ti one ($\Delta H_{max} = -17$ kJ mol^{-1}) [22]. These values of ΔH_{max} were calculated in terms of the Miedema model [23]. Thus, one can expect the FeZr amorphous phase to be formed more efficiently than the FeTi one. Our results show, however, that almost all Fe atoms experience amorphous short-range order (SRO) in the Fe/Ti multilayers with $\Lambda = 5$ nm whereas in the Fe/Zr multilayer system with $\Lambda = 5$ nm only about 35% of Fe atoms are contained in the amorphous phase.

3.2. X-ray diffraction measurements

The structure of the Fe/Ti multilayers was studied also by the XRD method. The XRD patterns recorded for the films with $\beta = 1$ and $\beta = 1.5$ are shown in figures 5(a) and 6(a), respectively. These results show that the Fe/Ti system is composed predominantly of closely

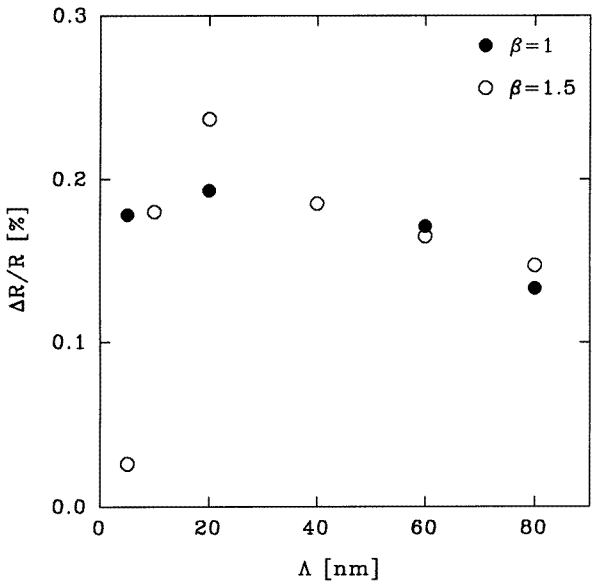

Figure 8. The magnetoresistivity versus the modulation wavelength Λ for $\beta = 1$ and $\beta = 1.5$.

packed (110) planes of bcc-Fe and (100) hcp-Ti. The plane spacings (d) calculated from the (110) Fe and (100) Ti peak positions were about 0.2028 nm and 0.2558 nm for Fe and Ti, respectively. The d-spacing in the Ti layers is smaller than the bulk value of the (100) hcp-Ti peak, with the maximum deviation of about 6% for $\Lambda \approx 60$ nm (figures 5(b), 6(b)). For Fe layers the d-spacing is almost independent of Λ for $\Lambda \geqslant 20$ nm but for $\Lambda < 20$ nm d decreases by about 1.7% as compared with the bulk value (figures 5(b), 6(b)).

The XRD measurements allowed determination of the size of the Fe and Ti crystallites (D_{Fe} and D_{Ti}) by using the Scherrer formula. For both film compositions the sizes of the Fe crystallites are comparable to d_{Fe}, while those of the Ti crystallites are systematically smaller than the corresponding values of d_{Ti} over the whole range of Λ (figures 5(c), 6(c)). For all Λ the average size of the Fe crystallites is larger than that of the Ti ones because of the grain boundary diffusion during which the Ti grains convert more quickly to the amorphous state than the Fe ones. This effect can be easily seen in the XRD patterns: the intensity of the (100) hcp-Ti peak decreases much faster than that of the (110) bcc-Fe peak (figures 5(a) and 6(a)) when the elemental layer thickness becomes smaller. The relative fractions of the crystalline bcc-Fe, hcp-Ti and amorphous FeTi phases were determined from the integrated intensities of the XRD lines corresponding to a given phase. The pseudo-Voigt shape of the diffraction peaks was used in the calculations [24]. The amorphous fraction determined in this way rapidly increases for decreasing Λ in good qualitative agreement with the CEMS results (figure 4). In the Fe/Ti multilayers with $\Lambda \geqslant 20$ nm the Fe and Ti layers are predominantly crystalline.

3.3. Magnetic measurements

The magnetic properties of the Fe/Ti multilayers were investigated using conventional techniques. The magnetization (M_s) and the coercive field (H_c) were determined from the hysteresis loop by using a vibrating-sample magnetometer (VSM). For $\beta = 1.5$ the

magnetization remains constant (about 0.065 T) for $\Lambda \geqslant 10$ nm and then rapidly decreases to less than 0.01 T for $\Lambda = 5$ nm (figure 7(a)). For $\beta = 1$ the magnetization exceeds that recorded for $\beta = 1.5$ over the whole range of Λ and similarly drastically decreases for $\Lambda = 5$ nm. The coercive field (H_c) is similar for both compositions (about 180 Oe) for $\Lambda \geqslant 20$ nm (figure 7(b)), and it decreases rapidly with decreasing Λ. For $\Lambda = 5$ nm, H_c is about 30 Oe and 75 Oe for $\beta = 1.5$ and $\beta = 1$, respectively. Such changes of M_s and H_c indicate the transition from the polycrystalline ($D_{\mathrm{Fe}} \sim 10$ nm) to the amorphous ($D_{\mathrm{Fe}} < 2$ nm) structure (figure 7). A similarly drastic decrease of the coercive field for small Λ was observed recently in the Fe/Zr [25] and Co/Ti [26] multilayer systems due to transformation from the crystalline to the amorphous state.

The anisotropic magnetoresistivity $\Delta R/R$ almost vanishes for the smallest value of Λ for film with $\beta = 1.5$, confirming that the Fe/Ti multilayer films with $\Lambda \leqslant 5$ nm are almost entirely amorphous (figure 8). However, $\Delta R/R$ for film with $\beta = 1$ and $\Lambda = 5$ nm does not vanish yet because this multilayer is not completely amorphous and still contains a considerable amount of the ferromagnetic α-Fe phase, as shown by the CEMS results (figures 1(e) and 4), which contribute to about 20% of the total spectral area.

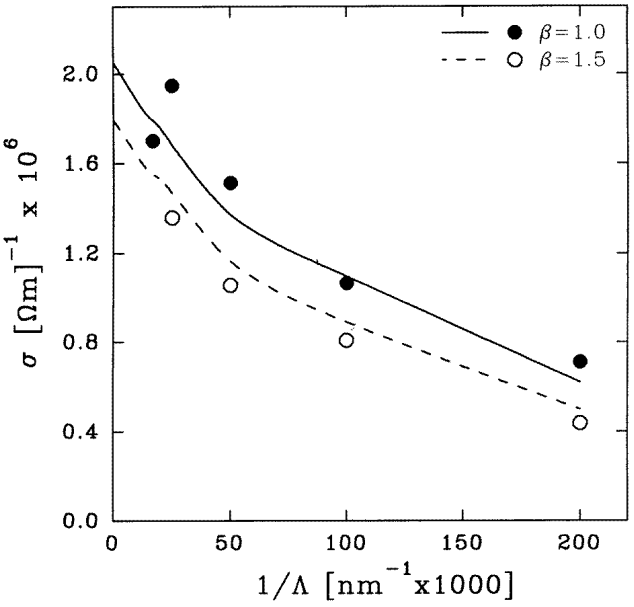

Figure 9. The electrical resistivity versus the reciprocal of the modulation wavelength Λ. The solid and dashed lines are calculated according to equation (3) in terms of the model discussed in the text.

The magnetic measurements were supplemented by the measurements of the electric conductivity as a function of the modulation wavelength. The electric conductivity σ versus $1/\Lambda$ is shown in figure 9. Our experimental data, which are similar to those reported by Rodmacq *et al* [12], were interpreted in terms of the model which assumes that the amorphous phase is formed during sputter deposition not only in the plane between the crystalline layers of Fe and Ti but also distributed in the grain boundaries due to diffusion in the grain boundaries being stronger than the volume diffusion [27]. The resulting electrical

conductivity is then

$$\sigma = \frac{\sigma_{am}}{\Lambda}[6Z_{Fe}(0) + F_{Fe}(d_{Fe} - 2Z_{Fe}(0)) + F_{Ti}(d_{Ti} - 4Z_{Fe}(0))] \tag{3}$$

where $Z_{Fe}(0) = 1$ nm is the initial thickness of the crystalline Fe sublayer which was reduced by the thickness of the amorphous interface sublayer.

$$F_i = \frac{R_i + 1 + f_i(1 - R_i)}{R_i + 1 - f_i(1 - R_i)} \tag{4}$$

is the crystallite distribution function where grains are in the form of very thin cylinders (the two-dimensional model) [28, 29] in sublayer i (i = Fe, Ti), $R_i = \rho_i/\rho_{am}$ ($\rho_{am} = 200\ \mu\Omega$ cm, $\rho_{Ti} = 130\ \mu\Omega$ cm, $\rho_{Fe} = 30\ \mu\Omega$ cm), and $f_i(L) = V_{i(C)}/V_{i(tot)}$ (determined from XRD and CEMS measurements) is the relative amount of crystalline phase in the crystalline sublayer i. If $f_i = 0$, then $\sigma = \sigma_{am}$; if $1/\Lambda \to 0$ and $f_i = 1$, then equation (3) transforms into one for a parallel connection of resistances and

$$\sigma = \frac{\beta\sigma_{Fe} + \sigma_{Ti}}{1 + \beta}. \tag{5}$$

The solid and dashed lines in figure 9, calculated by using equation (3), for $\beta = 1$ and $\beta = 1.5$, respectively, show good agreement with σ measured for $\Lambda \leqslant 40$ nm.

4. Conclusions

A detailed systematic investigation of the Fe/Ti multilayer system over a wide range of elemental layer thicknesses for two nominal compositions was performed by complementary techniques including the Mössbauer spectroscopy, x-ray diffraction, hysteresis loop, magnetoresistance and electric conductivity methods. From these measurements we can conclude that the Fe/Ti multilayers with $\Lambda \geqslant 10$ nm consist of predominantly crystalline Fe and Ti layers. The amorphous phase is formed during sputter deposition in the plane between crystalline sublayers as well as in the grain boundaries. The Fe/Ti multilayers with $\Lambda \leqslant 5$ nm are entirely amorphous. The spin orientation in Fe layers determined from CEMS measurements shows strong alignment in the plane of the film. However, in the spectral components corresponding to the interfacial regions, random spin orientation was observed. The thickness of the mixed interfacial region formed during the deposition process was determined.

Acknowledgments

The financial support from the Polish Committee for Scientific Research under grants No 2P03B 098 08 and No 7T08A 057 08 is gratefully acknowledged.

References

[1] Nakatani R, Hoshino K, Noguchi S and Sugito Y 1994 *Japan. J. Appl. Phys.* **33** 133
[2] Maeland A J 1985 *Proc. 5th Int. Conf. on Rapidly Quenched Metals (Würzburg, 1984)* ed S Steeb and H Warlimont (Amsterdam: North-Holland) p 1507
[3] Menzel D, Niklas A and Köster H 1991 *Mater. Sci. Eng.* A **133** 312
[4] Kopcewicz M and Williamson D L 1993 *J. Appl. Phys.* **74** 4363
[5] Kopcewicz M, Jagielski J, Stobiecki T, Stobiecki F and Gawlik G 1994 *J. Appl. Phys.* **76** 5232
[6] Wertheim G K, Wernick J H and Sherwood R C 1969 *Solid State Commun.* **7** 1399
[7] Mizuno T and Morozuni T *1982 J. Less-Common Met.* **84** 237

[8] Murray J L 1986 *Binary Alloy Phase Diagrams* vol 2, ed T B Massalski (Metals Park, OH: American Society for Metals) p 1117
[9] Sumiyama K, Hashimoto Y, Yoshikate T and Nakamura Y 1983 *J. Magn. Magn. Mater.* **31–34** 1495
[10] Liou S H and Chien C L 1984 *J. Appl. Phys.* **55** 1820
[11] Chien C L and Liou S H 1985 *Phys. Rev.* B **31** 8238
[12] Rodmacq B, Hillairet J, Laugier J and Chamberod A 1990 *J. Phys.: Condens. Matter* **2** 95
[13] Balogh J, Rodmacq B and Chamberod A 1988 *Solid State Commun.* **66** 143
[14] Brenier R, Thevenard P, Capra T, Perez A, Treilleux M, Romana L, Dupuy J and Brunel M 1987 *Nucl. Instrum. Meth.* B **19+20** 691
[15] Ray R, Giessen B C and Grant N J 1972 *Metall. Trans.* **3** 627
[16] Nakamura Y, Sumiyama K and Ezawa H 1986 *Hyperfine Interact.* **27** 361
[17] Kopcewicz M, Jagielski J, Gawlik G and Grabias A 1995 *J. Appl. Phys.* **78** 1312
[18] Hesse J and Rübartsch A 1974 *J. Phys. E: Sci. Instrum.* **7** 526
[19] LeCaer G and Dubois J M 1979 *J. Phys. E: Sci. Instrum.* **12** 1083
[20] Krebs H U, Webb D J and Marshall A F 1987 *Phys. Rev.* B **35** 5392
[21] Williamson D L and Clemens B 1988 *Hyperfine Interact.* **42** 967
[22] Hellstern E 1987 Glasbildung durch mechanisches Legieren *Dissertation* Konstanz University
[23] Miedema A R, de Chatel P R and de Boer F R 1980 *Physica* B **100** 1
[24] Czapkiewicz M, Stobiecki T and Kopcewicz M 1996 *J. Magn. Magn. Mater.* at press
[25] Czapkiewicz M and Stobiecki T 1995 *J. Magn. Magn. Mater.* **148** 333
[26] Chrzumnicka K, Dubowik J, Gontarz R, Gościańska I, Ratajczak H, Smardz L, Stobiecki F and Szymański B 1996 *J. Magn. Magn. Mater.* at press
[27] Otto T, Stobiecki T, Stobiecki F and Röll K 1991 *J. Magn. Magn. Mater.* **101** 207
[28] Mogro-Campero A and Walter J L 1980 *J. Physique Coll.* **41** C8 497
[29] Stobiecki F and Stobiecki T 1983 *J. Magn. Magn. Mater.* **40** 111